Article:
Karadakov, Peter Borislavov orcid.org/0000-0002-2673-6804 and Riley, Tom (2023) The Effect of Hydrogenation on the Contest between Aromaticity and Antiaromaticity in Norcorrole. Chemistry : A European Journal. e202203400. ISSN: 0947-6539

https://doi.org/10.1002/chem.202203400

Chemistry–A European Journal
Research Article
doi.org/10.1002/chem.202203400
Chemistry Europe
European Chemical Societies Publishing
www.chemeurj.org

The Effect of Hydrogenation on the Contest between Aromaticity and Antiaromaticity in Norcorrole

Peter B. Karadakov*[a] and Tom Riley[a]

Abstract: Magnetic shielding studies demonstrate that successive hydrogenation of Ni^{II} norcorrole (NiNc), a stable molecule combining aromatic and antiaromatic features, first weakens and then eliminates the central antiaromatic region, even though the NiNc antiaromatic "core", a 14-membered conjugated cycle with 16 π electrons, is formally preserved throughout the H_2NiNc–H_8NiNc series. The differences between aromatic and non-aromatic isotropic shielding distributions and nucleus-independent chemical shift (NICS) values in these hydrogenated porphyrin analogues are highlighted by comparing the results for the members of the H_2NiNc–H_8NiNc series to those for the aromatic Ni^{II} porphyrin complex. The results strongly support the unexpected and counterintuitive conclusion that H_8NiNc will be nonaromatic, without even a trace of antiaromaticity. Based on these findings, H_8NiNc is predicted to be the most stable member of the H_2NiNc–H_8NiNc series.

Introduction

Norcorrole (H_2Nc), a molecule which was initially proposed on the basis of DFT calculations,[1] is the smallest cyclic tetrapyrrole porphyrin analogue synthesized to date.[2–3] Magnetic shielding studies have demonstrated[4] that H_2Nc and its more popular Ni^{II} complex (NiNc) provide unusual examples of stable molecules with high antagonistic levels of antiaromaticity and aromaticity: Both molecules incorporate a deshielded antiaromatic "core", a 14-membered cyclic conjugated subsystem with 16 π electrons, surrounded by an aromatic "halo" in the form of increased shielding over a peripheral conjugated ring, which can be viewed either as a ring of 14 atoms and 14 π electrons involving two links through homoconjugation, or as a ring of 18 atoms with 18 π electrons. The biological importance of hydrogenated porphyrins such as chlorins, bacteriochlorins and isobacteriochlorins has prompted experimental interest in hydrogenated norcorroles.[5–6] Shinokubo and co-workers have reported Ni^{II} dihydronorcorrole (H_2NiNc) and Ni^{II} tetrahydronorcorrole (H_4NiNc) derivatives as the "first examples of antiaromatic porphyrinoids that contain saturated pyrrole units".[6] According to these authors, the ^{1}H NMR spectra of NiNc, H_2NiNc and H_4NiNc indicate that the antiaromatic features of the norcorrole π-system are gradually weakened upon hydrogenation over the pyrrole C_β–C_β bonds.[6] The disruption of the peripheral conjugated system in H_2NiNc and H_4NiNc can be expected to eliminate the aromatic shielded "halo" observed in NiNc. This could explain why H_2NiNc was found to be less stable than NiNc[6] but does not explain the stability of H_4NiNc and the ^{1}H NMR spectra of H_2NiNc and H_4NiNc[6] – without the aromatic "halo" both molecules should be not less but more antiaromatic. Another intriguing question is whether further hydrogenation over the pyrrole C_β–C_β bonds to produce Ni^{II} hexahydronorcorrole (H_6NiNc) and Ni^{II} octahydronorcorrole (H_8NiNc) will additionally weaken the antiaromatic features or even eliminate them completely, resulting in non-aromatic compounds – if so, this would be counterintuitive, as structural formulas (Figure 1) suggest that the 14-membered cyclic conjugated subsystem with 16 π electrons responsible for the NiNc antiaromatic "core" is formally preserved throughout the H_2NiNc–H_8NiNc series.

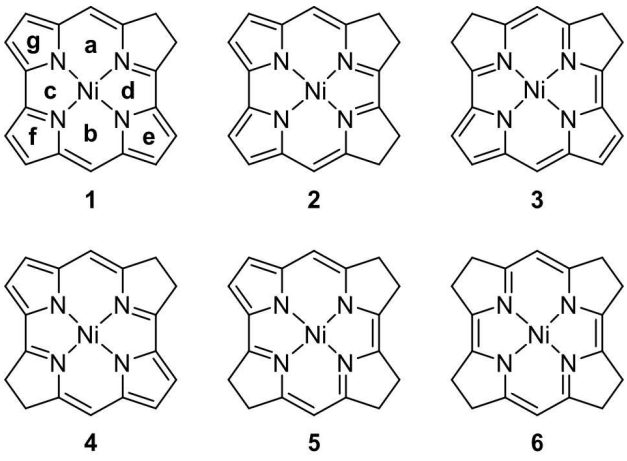

Figure 1. H_2NiNc **1**, H_4NiNc **2**–**4**, H_6NiNc **5** and H_8NiNc **6**. The letters **a**–**g** in **1** identify the 5- and 6-membered conjugated rings for which NICS were calculated.

[a] *Prof. Dr. P. B. Karadakov, T. Riley*
Department of Chemistry
University of York
Heslington, York YO10 5DD (UK)
E-mail: peter.karadakov@york.ac.uk

Supporting information for this article is available on the WWW under https://doi.org/10.1002/chem.202203400

In this paper we investigate the effect of successive hydrogenation on the levels of aromaticity and antiaromaticity in H_2NiNc, H_4NiNc, H_6NiNc and H_8NiNc by analyzing the spatial variations in off-nucleus isotropic magnetic shielding, $\sigma_{iso}(\mathbf{r}) = {}^1/_3[\sigma_{xx}(\mathbf{r}) + \sigma_{yy}(\mathbf{r}) + \sigma_{zz}(\mathbf{r})]$, within the molecular space of each of these hydrogenated norcorroles, and the changes in the values of the respective nucleus-independent chemical shifts (NICS)[7–9] for the 5- and 6-membered conjugated rings involving carbon, nitrogen and nickel atoms (Figure 1).

To highlight the differences between aromatic and non-aromatic isotropic shielding distributions and NICS values in porphyrin analogues, the results for the members of the H_2NiNc–H_8NiNc series are compared to those for the aromatic Ni^{II} porphyrin complex (NiP).

Computational Details

The geometries of H_2NiNc, H_4NiNc, H_6NiNc, H_8NiNc and NiP were optimized at the B3LYP-D3(BJ)/def2-TZVP level (B3LYP with Grimme's D3 empirical dispersion corrections and Becke–Johnson damping, within the def2-TZVP basis set, as implemented in GAUSSIAN[10]). In the case of H_4NiNc, all three isomers corresponding to different choices of the two pyrrole C_β–C_β bonds to be hydrogenated were investigated (**2**–**4** in Figure 1). All optimized geometries were confirmed as local minima through harmonic frequency calculations. The optimized geometries of all hydrogenated Ni^{II} norcorroles turned out to be bowl-shaped, those of H_2NiNc **1** and H_6NiNc **5** were found to have no point group symmetry, that of the lowest-energy isomer of H_4NiNc **4** has C_2 symmetry, the optimized geometries of the two higher-energy isomers of H_4NiNc **2** and **3** both have C_s symmetry and, finally, the optimized geometry of H_8NiNc **6** has C_{2v} symmetry (Figures S1 and S2). The lowest-energy isomer of H_4NiNc **4** corresponds to the Ni^{II} tetrahydronorcorrole derivative synthesized by Shinokubo and co-workers.[6]

At the B3LYP-D3(BJ)/def2-TZVP level the optimized geometry of NiP was found to be planar, of D_{4h} symmetry, with lowest vibrational frequency of just 8.5 cm^{-1} (B_{1u} normal mode) which indicates high flexibility with respect to a $D_{4h} \rightarrow D_{2d}$ distortion. In fact, according to earlier B3LYP/6-31G(d) studies[11–13] the D_{4h} geometry is a saddle point with a single imaginary frequency of 17*i* cm^{-1} (B_{1u} normal mode)[11] and the molecule assumes a "ruffled" D_{2d} geometry. The interplay between the D_{4h} and D_{2d} geometries for an octamethyl derivative of NiP (NiOMP) for different DFT methods and basis sets has been discussed in detail and compared to the experimental D_{2d} geometry obtained through a combination of gas-phase electron diffraction and mass spectrometry;[14] the conclusion was that most DFT methods favor the D_{4h} geometry when used with larger basis sets. For the purposes of the current investigation, it is more convenient to work with the planar D_{4h} geometry of NiP as it allows the construction of a $\sigma_{iso}(\mathbf{r})$ contour plot in the molecular plane. However, the $\sigma_{iso}(\mathbf{r})$ isosurfaces around NiP would remain qualitatively much the same if use was made of a geometry of D_{2d} symmetry.

$\sigma_{iso}(\mathbf{r})$ volume data required for the construction of isosurfaces and contour plots were obtained by means of B3LYP-GIAO/6-311++G(d,p) calculations [B3LYP with gauge-including atomic orbitals, within the 6-311++G(d,p) basis set], at the B3LYP-D3(BJ)/def2-TZVP optimized geometries of **1**–**6** and NiP. In all volume data calculations, $\sigma_{iso}(\mathbf{r})$ was evaluated on regular three-dimensional grids of points with a spacing of 0.1 Å. To reduce computational effort, for the grids enclosing **2**–**4**, **6** and NiP shielding tensors were calculated at the symmetry-unique points (using Abelian symmetry only) and then data were replicated by symmetry. For visualization purposes, all $\sigma_{iso}(\mathbf{r})$ values from the B3LYP-GIAO/6-311++G(d,p) calculations on **1**–**6** and NiP were assembled in GAUSSIAN cube files.[15]

NICS(0)[7] and NICS(1),[8–9] which measure $-\sigma_{iso}$(at the geometric ring center) and $-\sigma_{iso}$(at 1 Å above the geometric ring center), respectively, are straightforward to calculate for the planar D_{4h} geometry of NiP. Calculating NICS(0) for the non-planar geometries of **1**–**6** is also not a problem because the geometric center of each non-planar ring can still be located by averaging the coordinates of its atoms. One way of defining NICS(1) positions for non-planar rings which was used in the current work is to fit a plane to the ring atoms and ring center, and then use the points 1 Å above and below that plane along the normal passing through the ring center.[16] In general, these two points are not equivalent by symmetry and give two different NICS(±1) values. NICS values for **1**–**6** and NiP were calculated at the level of theory and geometries used to obtain $\sigma_{iso}(\mathbf{r})$ volume data.

Vertical excitation energies from the ground electronic state S_0 to low-lying singlet excited electronic states for NiNc, **1**–**6** and NiP were calculated at the TDB3LYP/def2-TZVP level, at the respective B3LYP-D3(BJ)/def2-TZVP optimized geometries.

All calculations reported in this paper were carried out in the gas phase and were performed using GAUSSIAN.[10] The Supporting Information includes figures showing all symmetry-unique bond lengths, natural population analysis (NPA) charges and nuclear isotropic shieldings for **1**–**6** and NiP, average bowl depths for **1**–**6**, additional computational details, energies, lowest vibrational frequencies and optimized geometries for **1**–**6**, NiP and pyrrolidine, as well as GAUSSIAN cube files with shielding data for **1**–**6** and NiP.

Results and Discussion

The $\sigma_{iso}(\mathbf{r})$ isosurfaces for **1**–**6** and NiP are shown in Figures 2 and 4a. The isovalues of $\sigma_{iso}(\mathbf{r}) = \pm 12$ ppm were chosen so as to provide optimal levels of detail and to allow comparisons to the isosurfaces for NiNc.[4] Isosurfaces for other isovalues can be inspected using the Gaussian cube files provided in the Supporting Information. The central deshielded region which **1** inherits from NiNc[4] is smaller in size than that in NiNc but it still dominates the central region (Figure 1). In the sequence **2**–**6** this region continues to shrink in size until it disappears completely in **6**, except for the close neighborhood of the Ni atom which remains deshielded even in NiP (Figure 3). This is a clear indication that the level of antiaromaticity decreases

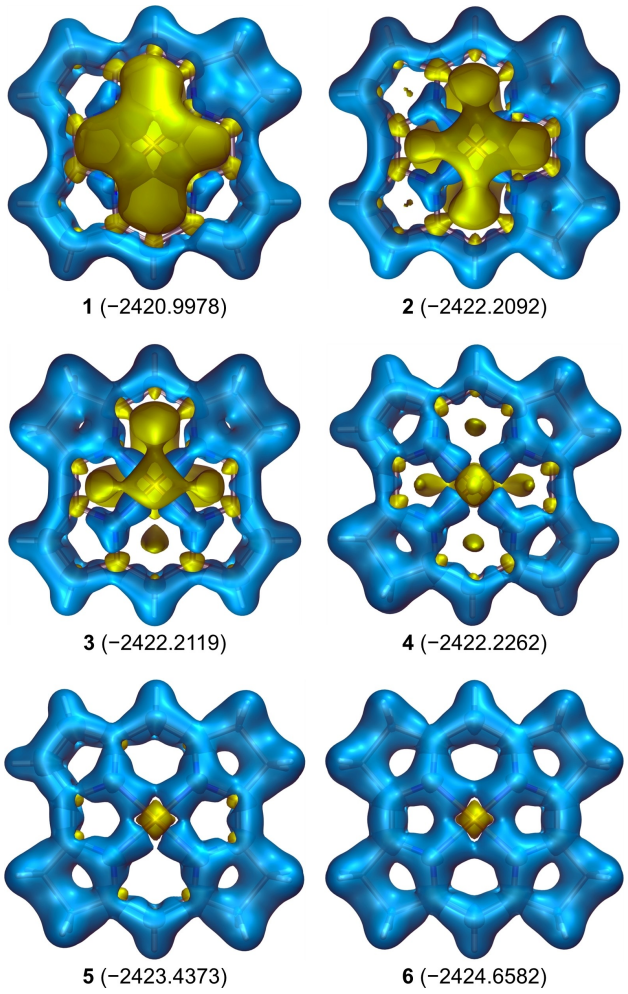

Figure 2. Shielding around **1**–**6** (views from above the top of each bowl). Isosurfaces at $\sigma_{iso}(\mathbf{r}) = +12$ ppm (shielded regions, blue) and $\sigma_{iso}(\mathbf{r}) = -12$ ppm (deshielded regions, yellow). The numbers in brackets correspond to the energies of the respective B3LYP-D3(BJ)/def2-TZVP optimized geometries (Ha).

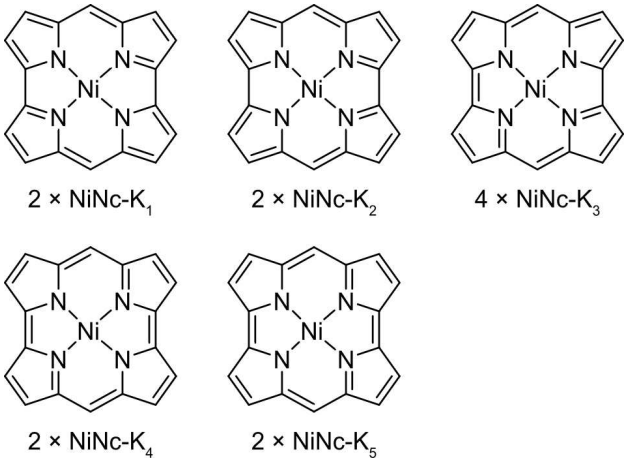

Figure 3. Kekulé resonance structures for NiNc (one structure of each type and the number of structures of the same type shown).

rapidly in the order **1**–**6**. On the other hand, the interior of NiP (Figure 4a) is much more shielded than that of **6** which suggests that, despite the absence of a central deshielded region and the significant shielding observed around all bonds, **6** is non-aromatic rather than aromatic.

The carbon and nitrogen atoms in **1**–**6** and NiP are surrounded by small ovoid deshielded regions inside which $\sigma_{iso}(\mathbf{r})$ becomes negative; such regions are also present in H_2Nc and NiNc.[4] Similar deshielding around sp^2 and sp hybridized carbon atoms and other sp^2 hybridized first main row atoms have been observed previously in conjugated rings,[17–19] as well

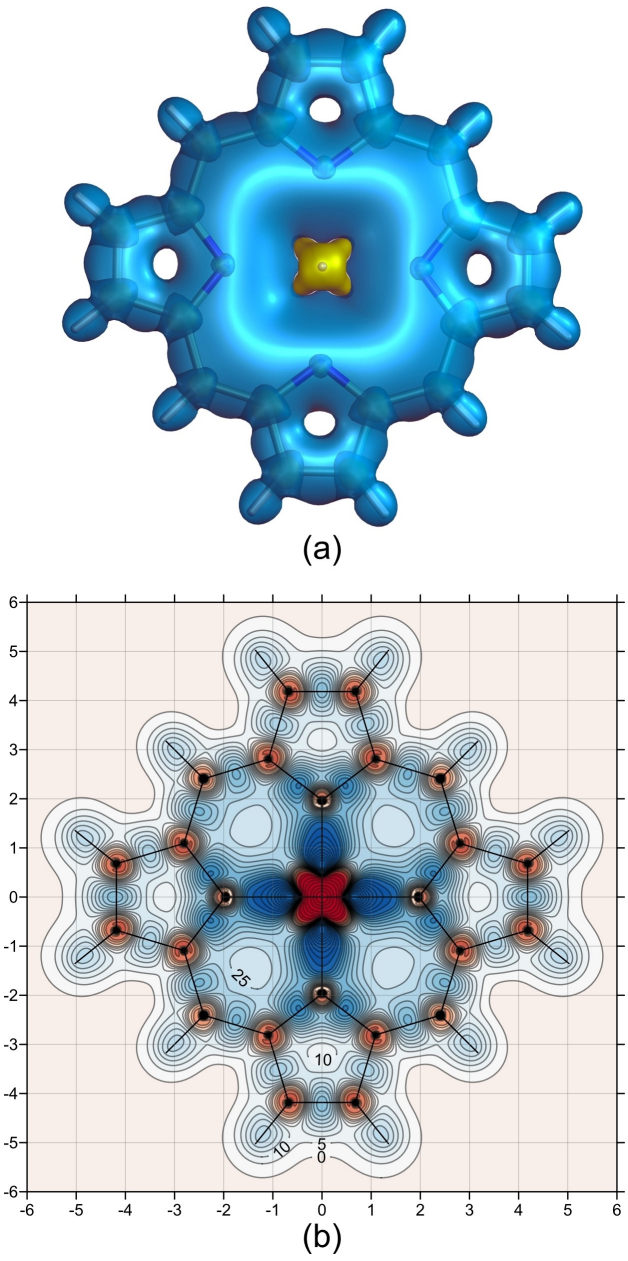

Figure 4. Shielding around NiP. (a) view from above, isosurfaces as in Figure 2; (b) contour plot in the molecular (horizontal) plane, contour levels in ppm (shielded and deshielded areas in blue and red, respectively), axes in Å. The energy of the B3LYP-D3(BJ)/def2-TZVP optimized geometry of NiP was obtained as −2497.3020 Ha.

as in open-chain and conjugated molecules such as ethene, ethyne and *s*-trans-1,3-butadiene.[20–21] These ovoid deshielded regions have been attributed to a specific type of π electron behavior characteristic of some sp^2 and sp hybridized first main row atoms that is different from traditional ring currents.[17] The occurrence of these deshielded regions around carbon and nitrogen atoms in H_2Nc, NiNc and **1**–**6** suggests that the hybridization states of these atoms are close to sp^2, as in NiP, despite the non-planar bowl-shaped geometries of these molecules. As a consequence, referring to the electrons involved in different bonds as (almost) π and σ electrons can be viewed as a reasonable approximation; this approximation is also supported by the shapes of the Kohn-Sham orbitals for **1**–**6**. The deshielded surroundings of Ni atoms which in **1**–**4** are submerged within larger deshielded regions are in line with the positive NPA charges on these atoms (Figure S1) and their negative isotropic shieldings (Figure S3).

Before discussing the $\sigma_{iso}(\mathbf{r})$ isosurfaces for the three isomers of H_4NiNc **2**–**4**, it is instructive to take a look at the 12 Kekulé resonance structures for NiNc, some of which are equivalent (Figure 3). The bowl-shaped NiNc is assumed to have 24 π electrons (18 from all carbons, 2 from each pyrrole-like nitrogen, and 1 from each pyridine-like nitrogen). Nickel is thought to make no contribution to the π system, but it is engaged in bonds to the nitrogen through the σ electron on each pyrrole-like nitrogen and the σ electron pair on each pyridine-like nitrogen. The resonance structure drawn most often in the literature for NiNc (and for other Nc compounds with an identical π system) is one of the NiNc-K_1 pair.[1–3,6, 22–26] NiNc-K_2 has been used as an alternative to NiNc-K_1 in association with $NiNc^{2-}$ [27–28] and a P^{V}Nc complex.[29] Structures NiNc-K_3, NiNc-K_4 and NiNc-K_5 treat one or both of the longer C_α–C_α bonds as "double" which is less realistic, but the number of structures of these types suggests that they can still make sizeable contributions to resonance in NiNc. In addition to the Kekulé resonance structures for NiNc (Figure 3), it is possible to draw a number of Dewar-style resonances structures with "diagonal" bonds[30] but, at the moment, establishing the relative importance of all of these resonance structures is not practically feasible because treating 24 π electrons is beyond the capabilities of suitable approaches such as spin-coupled generalized valence-bond (SCGVB) theory.[31] It is important to note that there are Kekulé resonance structures with "double" bonds that are placed so as to allow hydrogenation to each of **1**–**6**.

The central deshielded region in **1**, although smaller in size, resembles that in NiNc[4] and still extends over the same 14-membered cyclic conjugated subsystem with 16 π electrons. All C–C bonds along the perimeter of **1** are shielded to different extents, with higher shielding over the hydrogenated pyrrole unit and "pinch points" over two of the C_m–C_α bonds. The increased shielding over the hydrogenated pyrrole unit suggests some hyperconjugation[32] involving the C_β–H bonds. This is supported by a reduction in the C_α–C_β bond lengths in that unit, 1.503 Å and 1.519 Å (Figure S1), in comparison to the corresponding bond length in pyrrolidine, optimized in the gas-phase at the same level of theory, 1.537 Å. Similar evidence of hyperconjugation is observed in **2**–**6**. The perimeters of **2**–**6** are also shielded, to different extents, and still without disruptions in the $\sigma_{iso}(\mathbf{r}) = 12$ ppm isosurfaces. Thus, contrary to expectations, hydrogenation over one or more pyrrole C_β–C_β bonds in NiNc does not eliminate the shielded "halo", although the "halo" should no longer be referred to as "aromatic" because it is not straightforward to count the number of electrons producing this effect. The variations in isotropic shielding around **1** indicate that antiaromatic destabilization from the central deshielded region and stabilization from the shielded periphery are both weakened in comparison to NiNc[4] but do not show a visually observable change in the balance between these effects which would explain why H_2NiNc was found to be less stable than NiNc.[6]

The H_4NiNc isomers **2**–**4** provide a unique example of a direct link between stability and level of antiaromaticity. The deshielded antiaromatic "core" in the highest-energy isomer **2** is significantly larger than that in **3**; that deshielded "core" has all but disappeared in the lowest-energy isomer **4**. The shielded "halos" along the peripheries of **2** and **3** are thicker than that around **4**, but not sufficiently so as to counteract the antiaromaticities of the respective central regions and change the energy ordering (from the data shown in Figure 2, the energy differences between **2** and **3**, and **3** and **4** amount to ca. −7 and −37 kJ mol^{-1}, respectively).

The $\sigma_{iso}(\mathbf{r}) = \pm 12$ ppm isosurfaces for H_6NiNc **5** suggest that any remaining antiaromatic character is much less than that in **4**. However, decreasing the negative isovalue to $\sigma_{iso}(\mathbf{r}) = -10$ ppm leads to the appearance of small deshielded regions near the centers of two of the four five- and six-membered rings involving Ni; at $\sigma_{iso}(\mathbf{r}) = -4$ ppm deshielded regions appear within the interiors of all four rings involving Ni (the $\sigma_{iso}(\mathbf{r}) = -10$ ppm and $\sigma_{iso}(\mathbf{r}) = -4$ ppm isosurfaces can be examined using the Gaussian cube files provided in the Supporting Information). This shows that **5**, although less antiaromatic than **4**, still retains a low level of antiaromaticity.

While shielding around H_8NiNc **6** can viewed as an enhanced version of that around **5**, there is an important feature that is now fully developed: The 14-membered cyclic conjugated subsystem sustaining the antiaromatic "core" in NiNc is now interconnected by well-shielded bonds which is an indication that it is no longer antiaromatic. This is further supported by the observation that deshielded regions do not appear within the interiors of the four rings involving Ni even if the negative isovalue is decreased to $\sigma_{iso}(\mathbf{r}) = -1$ ppm.

We note that with the decrease of the level of antiaromaticity of the central region in **1**–**6**, the Ni–N bonds become more shielded. This is an indication of strong bonding interactions and, possibly, additional conjugation pathways across the N–Ni–N links.

In this paper NiP is used as an aromatic reference point to help find out whether the gradual decrease in antiaromaticity upon successive hydrogenation of NiNc in the sequence **1**–**6** is sufficient to produce an aromatic fully hydrogenated H_8NiNc **6**. Aromaticity in porphyrins has been studied using a wide range of theoretical approaches,[33–41] and the current results on NiP, while generally in agreement with the results of other authors, highlight several important details. According to the $\sigma_{iso}(\mathbf{r}) = +$

12 ppm isosurface and the $\sigma_{iso}(\mathbf{r})$ contour plot in the molecular plane in Figure 4 the most shielded region in NiP is that around the "internal cross",[33] a ring of 16 atoms with 18 π electrons. The four pyrrole rings are relatively less shielded which suggests that even though these rings make some contribution to the aromaticity of NiP, the more significant contribution comes from the "internal cross". The $\sigma_{iso}(\mathbf{r})$ contour plot in the molecular plane (Figure 3b) shows that the Ni–N bonds are very well shielded, with $\sigma_{iso}(\mathbf{r})$ values reaching ca. 170 ppm, much more so than C–N and C–C bonds, for which the $\sigma_{iso}(\mathbf{r})$ values do not exceed ca. 66 ppm and ca. 46 ppm, respectively. According to the results of a natural bond orbital (NBO) analysis,[42] the Ni–N interactions in NiP are the result of electronic delocalization of sp^2 lone pairs on the nitrogen atoms into a 3d orbital on the nickel atom. However, the shielding around Ni–N bonds is much higher than what could be expected from this model. Its interpretation requires a better understanding of how the electrons on Ni contribute to the overall shielding picture than that afforded by the current calculations.

Even though all bonds within the smaller "internal cross" made up of rings **a**–**d** in **6** are well-shielded (Figure 2), each of these rings has a sizeable central "hole" in the $\sigma_{iso}(\mathbf{r}) = +12$ ppm isosurface; such "holes" are not present in any of the rings from the "internal cross" of NiP (Figure 4). To allow a more detailed comparison between the shielding distributions above and below **6** and NiP, we constructed shielding contour plots in vertical planes for both molecules (Figure 5). Each of these vertical planes passes through the principal axis of symmetry and through the N–Ni–N sequence from two opposite Ni–N bonds; for NiNc this plane corresponds to one of the two σ_v symmetry planes.

As shown in Figure 5, in NiP the shielded regions above and below the molecular plane extend significantly further than the corresponding regions outside and inside the bowl in **6**. This is most noticeable in the $\sigma_{iso}(\mathbf{r}) = +5$ ppm isoline which passes ca. 3.3 Å above and below the molecular plane of NiP, and just ca. 1.5 Å above and ca. 1.2 Å below the bowl in **6**. These observations provide further support for the conclusion that **6** is non-aromatic rather than aromatic. The Ni–N bonds in **6** are well shielded but less so than those in NiP, with $\sigma_{iso}(\mathbf{r})$ values reaching ca. 122 ppm. The oval shielded regions to the left and to the right of the N–Ni–N bonds in **6** (Figure 5a) and the respective kidney-shaped regions in NiP (Figure 5b) illustrate the changes in shielding around the points at which the vertical planes cut through opposite C_β–C_β bonds. The near-circular shielding distributions around these points in **6** indicate that the C_β–C_β bonds in **6** are very much single σ bonds; the respective kidney-shaped shielding distributions observed in NiP indicate that the C_β–C_β bonds in NiP have significant π character, not dissimilar to that in the C–C bonds in benzene.[43]

Clearly, the shielding isosurfaces and contour plots in Figures 2, 4 and 5 contain much more information than single-point NICS. However, it is still interesting to investigate the extent to which NICS can reproduce the aromaticity trends in NiNc, **1**–**6** and NiP. The NICS(0) and NICS($\pm$1) values for these molecules are collected in Table 1 (NiNc and NiP have one

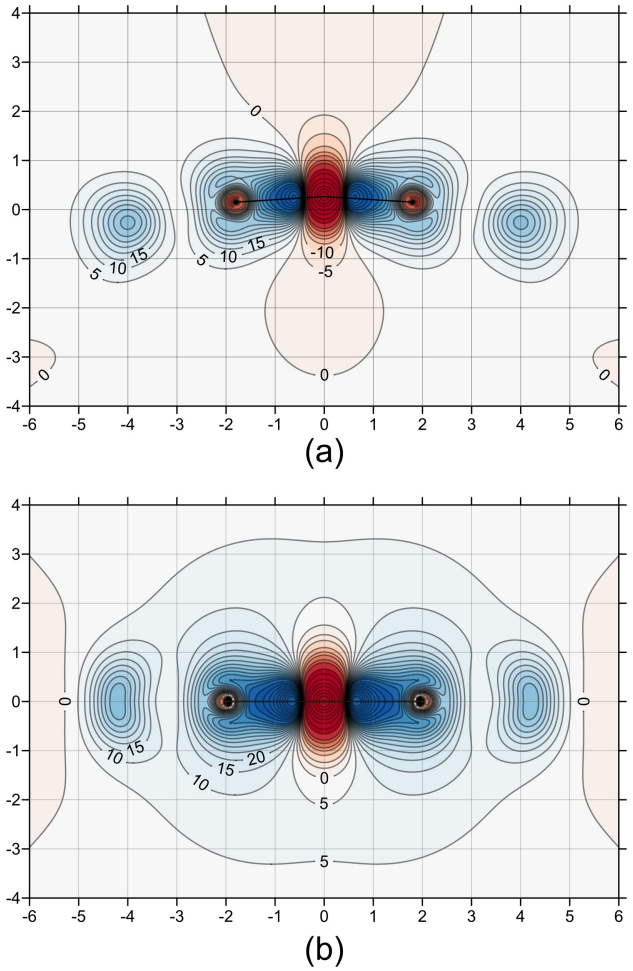

Figure 5. $\sigma_{iso}(\mathbf{r})$ contour plots for (a) **6** and (b) NiP in vertical planes centered on the Ni atom and passing through the N–Ni–N atoms in two opposite Ni–N bonds. Details as for Figure 4b.

additional pyrrole ring each, with NICS values identical to those for the other pyrrole rings). According to the NICS values for rings **a**–**d**, even in **1** these rings are significantly less antiaromatic than they are in NiNc. The decrease in the antiaromaticity of rings **a**–**d** continues in the sequence **2**–**5**, in parallel for all four rings, with a single exception: Ring **a** in **3** is slightly more antiaromatic than its counterpart in **2**, but the lower levels of antiaromaticity in rings **b**–**d** leave no doubt that **3** is less antiaromatic than **2**. When we come to **6**, most of the NICS values for rings **a**–**d** become negative but of very low magnitudes which supports the conclusion that **6** is non-aromatic. The pyrrole rings (**e**–**g** in **1**) show moderate to low levels of antiaromaticity in NiNc, **1**–**3** and become nonaromatic in **4** and **5**.

We show in Table 2, for each of NiNc, **1**–**6** and NiP, the vertical excitation energy ΔE between the ground electronic state S_0 and the lowest singlet excited electronic state dominated by the HOMO→LUMO orbital excitation. For NiNc and **1**–**6** this state is the first singlet excited state S_1, and for NiP it is the doubly degenerate third singlet excited state S_3 (S_1 and the doubly degenerate S_2 are dominated by orbital excitations

Table 1. NICS(0) and NICS(±1) values (in ppm) for NiNc (from Ref. [4]), **1**–**6** and NiP. NICS(+1) and NICS(−1) for NiNc and **1**–**6** correspond to locations outside and inside the bowl, respectively. For ring labels, see Figure 1; in some of the molecules certain rings are equivalent by symmetry.

Molecule/Ring		a	b	c	d	e	f	g
NiNc	NICS(+1)	37.0	=**a**	36.9	=**c**	2.8	=**e**	=**e**
	NICS(0)	49.5	=**a**	49.6	=**c**	8.1	=**e**	=**e**
	NICS(−1)	45.7	=**a**	48.2	=**c**	12.3	=**e**	=**e**
1	NICS(+1)	23.4	24.4	24.3	26.0	−1.4	4.0	3.9
	NICS(0)	31.7	33.1	32.3	36.1	1.9	9.5	8.8
	NICS(−1)	29.6	30.4	32.6	35.1	5.9	10.0	11.4
2	NICS(+1)	17.9	=**a**	17.3	24.3	–	6.8	=**f**
	NICS(0)	25.0	=**a**	21.6	32.9	–	12.3	=**f**
	NICS(−1)	23.2	=**a**	22.8	32.4	–	11.3	=**f**
3	NICS(+1)	18.3	10.2	16.5	=**c**	2.4	=**e**	–
	NICS(0)	26.2	13.5	20.9	=**c**	6.1	=**e**	–
	NICS(−1)	23.2	13.1	21.9	=**c**	5.4	=**e**	–
4	NICS(+1)	9.6	=**a**	10.9	=**c**	−1.8	–	=**e**
	NICS(0)	12.8	=**a**	13.9	=**c**	0.3	–	=**e**
	NICS(−1)	11.5	=**a**	14.4	=**c**	0.8	–	=**e**
5	NICS(+1)	2.8	6.8	5.5	6.6	–	–	0.2
	NICS(0)	3.5	9.7	5.4	7.0	–	–	2.6
	NICS(−1)	3.5	8.1	6.9	8.7	–	–	0.7
6	NICS(+1)	−0.4	=**a**	0.0	=**c**	–	–	–
	NICS(0)	−0.4	=**a**	−2.4	=**c**	–	–	–
	NICS(−1)	−0.4	=**a**	0.2	=**c**	–	–	–
NiP	NICS(1)	−18.0	=**a**	–	–	−9.4	=**e**	=**e**
	NICS(0)	−21.7	=**a**	–	–	−6.1	=**e**	=**e**

Table 2. Vertical excitation energies ΔE (eV) between the ground electronic state S_0 and the lowest singlet excited electronic state dominated by the HOMO→LUMO orbital excitation. For further details, see text.

Molecule	Transition	ΔE
NiNc	$S_1 \leftarrow S_0$	0.768
1	$S_1 \leftarrow S_0$	0.878
2	$S_1 \leftarrow S_0$	0.900
3	$S_1 \leftarrow S_0$	1.012
4	$S_1 \leftarrow S_0$	1.360
5	$S_1 \leftarrow S_0$	1.455
6	S1←S0	2.115
NiP	S3←S0	2.498

between orbitals other than the HOMO and LUMO). The vertical excitation energies increase in the order NiNc, **1**–**6**, NiP which provides further support for the aromaticity trends in these molecules established through the analysis of the isotropic shielding isosurfaces and NICS values.

Although obtaining accurate $\sigma_{iso}(^1H)$ values was not amongst the aims of the current study, we note that our lower pyrrole proton shieldings for **2** and **4** (Figure S3), in comparison to those calculated at the same level of theory for NiNc,[4] are in line with the respective downfield shifts of proton signals observed in substituted derivatives of NiNc, **2** and **4**.[6]

Conclusions

As shown in this paper, through a combination between a visual approach in which bonding and aromaticity are inspected using isotropic magnetic shielding isosurfaces and contour plots, and calculations of NICS and vertical singlet excitation energies, successive hydrogenation over the pyrrole C_β–C_β bonds in Ni^{II} norcorrole gradually weakens and then eliminates the central antiaromatic region. The final fully hydrogenated species, H_8NiNc, is predicted to be nonaromatic, without even a trace of antiaromaticity. These successive changes are somewhat counterintuitive because all members of the H_2NiNc–H_8NiNc series retain the 14-membered cyclic conjugated subsystem with 16 π electrons sustaining the antiaromatic "core" in NiNc. The nonaromatic character of H_8NiNc, established by comparing its magnetic shielding description, NICS and vertical singlet excitation energy to those of the aromatic Ni^{II} porphyrin, is unexpected for a system with $4n$ π electrons in its ground electronic state.

Similarly to the way in which H_2Nc was initially proposed on the basis of DFT calculations,[1] and synthesized later,[2–3] we expect that the current work will encourage the synthesis and experimental investigation of H_8NiNc, an unusual molecule which despite having a cyclic conjugated systems with 16 π electrons is not antiaromatic and is predicted to be the most stable member of the series of hydrogenated Ni^{II} norcorroles H_2NiNc–H_8NiNc.

Acknowledgements

We are grateful for the support of this work by the University of York.

Conflict of Interest

The authors declare no conflict of interest.

Data Availability Statement

The data that support the findings of this study are available from the corresponding author upon reasonable request.

Keywords: Aromaticity · hydrogenated norcorrole · norcorrole · nucleus independent chemical shifts · magnetic shielding

[1] A. Ghosh, I. H. Wasbotten, W. Davis, J. C. Swarts, *Eur. J. Inorg. Chem.* **2005**, 4479–4485.
[2] M. Bröring, S. Köhler, C. Kleeberg, *Angew. Chem. Int. Ed.* **2008**, *47*, 5658–5660; *Angew. Chem.* **2008**, *120*, 5740–5743.
[3] T. Ito, Y. Hayashi, S. Shimizu, J.-Y. Shin, N. Kobayashi, H. Shinokubo, *Angew. Chem. Int. Ed.* **2012**, *51*, 8542–8545; *Angew. Chem.* **2012**, *124*, 8670–8673.
[4] P. B. Karadakov, *Org. Lett.* **2020**, *22*, 8676–8680.
[5] B. Liu, X. Li, M. Stępień, P. J. Chmielewski, *Chem. Eur. J.* **2015**, *21*, 7790–7797.

[6] R. Nozawa, K. Yamamoto, I. Hisaki, J.-Y. Shin, H. Shinokubo, *Chem. Commun.* **2016**, *52*, 7106–7109.
[7] P. v. R. Schleyer, C. Maerker, A. Dransfeld, H. Jiao, N. J. R. v. E. Hommes, *J. Am. Chem. Soc.* **1996**, *118*, 6317–6318.
[8] P. v. R. Schleyer, H. Jiao, N. J. R. v. E. Hommes, V. G. Malkin, O. Malkina, *J. Am. Chem. Soc.* **1997**, *119*, 12669–12670.
[9] H. Fallah-Bagher-Shaidaei, C. S. Wannere, C. Corminboeuf, R. Puchta, P. v. R. Schleyer, *Org. Lett.* **2006**, *8*, 863–866.
[10] Gaussian 16 (Revision A.03), M. J. Frisch, G. W. Trucks, H. B. Schlegel, G. E. Scuseria, M. A. Robb, J. R. Cheeseman, G. Scalmani, V. Barone, G. A. Petersson, H. Nakatsuji, X. Li, M. Caricato, A. V. Marenich, J. Bloino, B. G. Janesko, R. Gomperts, B. Mennucci, H. P. Hratchian, J. V. Ortiz, A. F. Izmaylov, J. L. Sonnenberg, Williams, F. Ding, F. Lipparini, F. Egidi, J. Goings, B. Peng, A. Petrone, T. Henderson, D. Ranasinghe, V. G. Zakrzewski, J. Gao, N. Rega, G. Zheng, W. Liang, M. Hada, M. Ehara, K. Toyota, R. Fukuda, J. Hasegawa, M. Ishida, T. Nakajima, Y. Honda, O. Kitao, H. Nakai, T. Vreven, K. Throssell, J. A. Montgomery Jr., J. E. Peralta, F. Ogliaro, M. J. Bearpark, J. J. Heyd, E. N. Brothers, K. N. Kudin, V. N. Staroverov, T. A. Keith, R. Kobayashi, J. Normand, K. Raghavachari, A. P. Rendell, J. C. Burant, S. S. Iyengar, J. Tomasi, M. Cossi, J. M. Millam, M. Klene, C. Adamo, R. Cammi, J. W. Ochterski, R. L. Martin, K. Morokuma, O. Farkas, J. B. Foresman, D. J. Fox, Wallingford, CT, **2016**.
[11] P. M. Kozlowski, T. S. Rush, A. A. Jarzecki, M. Z. Zgierski, B. Chase, C. Piffat, B.-H. Ye, X.-Y. Li, P. Pulay, T. G. Spiro, *J. Phys. Chem. A* **1999**, *103*, 1357–1366.
[12] P. M. Kozlowski, J. R. Bingham, A. A. Jarzecki, *J. Phys. Chem. A* **2008**, *112*, 12781–12788.
[13] J. Barbee, A. E. Kuznetsov, *Comput. Theor. Chem.* **2012**, *981*, 73–85.
[14] A. E. Pogonin, A. A. Otlyotov, Y. Minenkov, A. S. Semeikin, Y. A. Zhabanov, S. A. Shlykov, G. V. Girichev, *Int. J. Mol. Sci.* **2022**, *23*, 320(1–17).
[15] See https://gaussian.com/cubegen/ (accessed 2 November 2022). .
[16] J. C. Dobrowolski, P. F. J. Lipiński, *RSC Adv.* **2016**, *6*, 23900–23904.
[17] P. B. Karadakov, P. Hearnshaw, K. E. Horner, *J. Org. Chem.* **2016**, *81*, 11346–11352.
[18] K. E. Horner, P. B. Karadakov, *J. Org. Chem.* **2013**, *78*, 8037–8043.
[19] K. E. Horner, P. B. Karadakov, *J. Org. Chem.* **2015**, *80*, 7150–7157.
[20] P. B. Karadakov, K. E. Horner, *J. Chem. Theory Comput.* **2016**, *12*, 558–563.
[21] P. B. Karadakov, J. Kirsopp, *Chem. Eur. J.* **2017**, *23*, 12949–12954.
[22] T. Yonezawa, S. A. Shafie, S. Hiroto, H. Shinokubo, *Angew. Chem. Int. Ed.* **2017**, *56*, 11822–11825; *Angew. Chem.* **2017**, *129*, 11984–11987.
[23] J. Conradie, C. Foroutan-Nejad, A. Ghosh, *Sci. Rep.* **2019**, *9*, 4852(1–6).
[24] M. Yamashina, Y. Tanaka, R. Lavendomme, T. K. Ronson, M. Pittelkow, J. R. Nitschke, *Nature* **2019**, *574*, 511–515.
[25] R. Nozawa, J. Kim, J. Oh, A. Lamping, Y. Wang, S. Shimizu, I. Hisaki, T. Kowalczyk, H. Fliegl, D. Kim, H. Shinokubo, *Nat. Commun.* **2019**, *10*, 3576(1–7).
[26] S.-Y. Liu, T. Fukuoka, N. Fukui, J.-Y. Shin, H. Shinokubo, *Org. Lett.* **2020**, *22*, 4400–4403.
[27] J.-Y. Shin, T. Yamada, H. Yoshikawa, K. Awaga, H. Shinokubo, *Angew. Chem. Int. Ed.* **2014**, *53*, 3096–3101; *Angew. Chem.* **2014**, *126*, 3160–3165.
[28] Z. Deng, X. Li, M. Stępień, P. J. Chmielewski, *Chem. Eur. J.* **2016**, *22*, 4231–4246.
[29] T. Yoshida, S. A. Shafie, H. Kawashima, N. Fukui, H. Shinokubo, *Org. Lett.* **2021**, *23*, 2826–2830.
[30] P. B. Karadakov, D. L. Cooper, B. J. Duke, J. Li, *J. Phys. Chem. A* **2012**, *116*, 7238–7244.
[31] T. H. Dunning, L. T. Xu, D. L. Cooper, P. B. Karadakov, *J. Phys. Chem. A* **2021**, *125*, 2021–2050.
[32] I. V. Alabugin, G. dos Passos Gomes, M. A. Abdo, *WIREs Comput. Mol. Sci.* **2019**, *9*, e1389(1–66).
[33] M. K. Cyrañski, T. M. Krygowski, M. Wisiorowski, N. J. R. van Eikema Hommes, P. v. R. Schleyer, *Angew. Chem. Int. Ed.* **1998**, *37*, 177–180; *Angew. Chem.* **1998**, *110*, 187–190.
[34] J. Jusélius, D. Sundholm, *Phys. Chem. Chem. Phys.* **1999**, *1*, 3429–3435.
[35] J. Jusélius, D. Sundholm, *Phys. Chem. Chem. Phys.* **2000**, *2*, 2145–2151.
[36] J. Jusélius, D. Sundholm, *J. Org. Chem.* **2000**, *65*, 5233–5237.
[37] R. W. A. Havenith, A. J. H. M. Meijer, B. J. Irving, P. W. Fowler, *Mol. Phys.* **2009**, *107*, 2591–2600.
[38] N. Otero, S. Fias, S. Radenković, P. Bultinck, A. M. Graña, M. Mandado, *Chem. Eur. J.* **2011**, *17*, 3274–3286.
[39] H. Fliegl, D. Sundholm, *J. Org. Chem.* **2012**, *77*, 3408–3414.
[40] J. I. Wu, I. Fernández, P. v. R. Schleyer, *J. Am. Chem. Soc.* **2013**, *135*, 315–321.
[41] E. Kleinpeter, A. Koch, S. Schulz, P. Wacker, *Tetrahedron* **2014**, *70*, 9230–9239.
[42] C. Berríos, G. I. Cárdenas-Jirón, J. F. Marco, C. Gutiérrez, M. S. Ureta-Zañartu, *J. Phys. Chem. A* **2007**, *111*, 2706–2714.
[43] P. B. Karadakov, K. E. Horner, *J. Phys. Chem. A* **2013**, *117*, 518–523.

Manuscript received: November 2, 2022
Accepted manuscript online: November 27, 2022
Version of record online: ■■, ■■■

RESEARCH ARTICLE

Off-nucleus isotropic shielding isosurfaces computed using DFT show that a key feature of Ni^{II} norcorrole (NiNc), its antiaromatic "core", a 14-membered cyclic conjugated subsystem with 16 π electrons that is formally preserved in all hydrogenated norcorroles, unexpectedly becomes less and less antiaromatic in the series H_2NiNc–H_8NiNc, which is predicted to end in the completely nonaromatic H_8NiNc.

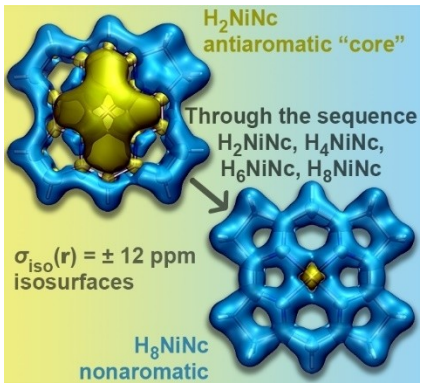

Prof. Dr. P. B. Karadakov, T. Riley*